



## Optically and thermally driven huge lattice orbital and spin angular momenta from spinning fullerenes

G. P. Zhang <sup>\*</sup>*Department of Physics, Indiana State University, Terre Haute, Indiana 47809, USA*

Y. H. Bai

*Office of Information Technology, Indiana State University, Terre Haute, Indiana 47809, USA*Thomas F. George *Department of Chemistry and Biochemistry and Department of Physics and Astronomy, University of Missouri–St. Louis, St. Louis, Missouri 63121, USA* (Received 12 May 2021; revised 15 July 2021; accepted 23 August 2021; published 7 September 2021)

Lattice vibration in solids may carry angular momentum. But unlike the intrinsic spin of electrons, the lattice vibration is rarely rotational. To induce angular momentum, one needs to find a material that can accommodate a twisted normal mode, two orthogonal modes, or excitation of magnons. If excitation is too strong, one may exceed the Lindemann limit, so the material melts. Therefore these methods are not ideal. Here, we theoretically propose a route to phonon angular momentum in a molecular crystal  $C_{60}$ . We find that a single laser pulse is able to inject a significant amount of angular momentum to  $C_{60}$ , and the momentum transfer is helicity dependent. Changing from right-circularly polarized light to left-circularly polarized light switches the direction of phonon angular momentum. On the ultrafast timescale, the orbital angular momentum change closely resembles the dispersive excitation of coherent phonons, with a cosine-function dependence on time, different from the spin counterpart. Atomic displacements, even under strong laser excitation, remain far below the Lindemann criterion. Under thermal excitation, spinning  $C_{60}$  even at room temperature generates a huge angular momentum close to several hundred  $\hbar$ . Our finding opens the door to a large group of fullerenes, from  $C_{60}$ ,  $C_{70}$  to their endohedral derivatives, where angular momentum can be generated through light or temperature. This paves the way to the phononic control electronic spin and harvesting thermal energy through phonon angular momentum.

DOI: [10.1103/PhysRevB.104.L100302](https://doi.org/10.1103/PhysRevB.104.L100302)

Nuclear vibration is ubiquitous and important to biological, chemical, and physical processes, ranging from photosynthesis [1], photoisomerization [2], to spin manipulation [3–5]. Microscopically, each material has its own vibrational normal modes. However, due to the symmetry constraint [6], normal modes rarely have a rotational eigenvector, so the phonon angular momentum (PAM) is feeble. The concept of phonon spin is not new [7,8], and reemerged [9]. McLellan [10] investigated PAM in a rotationally invariant harmonic model. Interest in PAM is more recent [9,11–14]. It was shown that one may use an electric field [15] or temperature gradient [16] to control PAM. By coupling PAM to the electronic spin degrees of freedom, one can use PAM to control spin devices [17]. However, the main obstacle is how to generate PAM in the first place. It was predicted that one could introduce chiral phonons in monolayer molybdenum disulfide [18], but the real calculation [19] showed that the effect is tiny in transition metal dichalcogenides. The same thing is true for  $Pt_3$  and  $Pt_5$  [20], where the majority of vibrational modes has nearly zero angular momentum, with the maximum close to  $0.094(\hbar/2)$ . Experimentally, it was demonstrated that

one could construct a superimposed vibrational state which consists of two orthogonal vibrational modes to generate an artificial circular phonon mode [21]. One may also couple the phonon to magnons in a magnetic material [22–25] to induce spin angular momentum of phonons, but one must first have magnons. In general, these methods are not easy.

Molecular crystals are different. The weak bonding between neighboring sites render atom motifs rotating freely. Buckminsterfullerene  $C_{60}$  [26] is a prime example. At room temperature,  $C_{60}$  is spinning rapidly [27–29] around its equilibrium lattice positions. Spinning is temperature dependent. As the temperature cools down below 261 K, the rotation slows down, where  $^{13}C$  NMR spectra of solid  $C_{60}$  show a significant broadening at a chemical shift of 143 ppm [27,30,31]. Its rotation can also be manipulated through substrates [32,33], the tip of a scanning tunneling microscope [34], and encapsulation inside carbon nanotubes [35].  $C_{60}$  rotation also affects its energy spectrum [36] and vibrational spectra [37].  $C_{60}$  and  $C_{70}$  are not the only fullerenes that spin. Endohedral fullerenes [38], with additional atoms encapsulated inside fullerenes, offer additional kinds of rotational dynamics [39], with applications to organic photovoltaic devices [40] and quantum computing [41]. Recently, possible light-induced superconductivity was reported in  $K_3C_{60}$  [42].

<sup>\*</sup>guo-ping.zhang@outlook.com

It is conceivable that light can inject angular momentum into  $K_3C_{60}$ . These readily available molecular crystals represent a new frontier for phonon angular momentum investigation.

In this Letter, instead of relying on artificial rotational motion of atoms to search for phonon angular momentum, we start with a material that rotates in the first place at room temperature. Specifically, we employ  $C_{60}$  as an example, and we show that a laser pulse can induce a significant orbital and spin angular momentum change. PAM depends on the laser helicity. Circularly polarized light injects more angular momentum into the system than linearly polarized light. Changing from right- to left-circularly polarized light switches angular momentum direction. The total angular momentum exactly follows the energy change, thus reaffirming that it is physical. The orbital and spin angular momenta depend on time differently. The orbital has a cosine dependence, very similar to dispersive excitation of coherent phonons [43]. The lattice distortion of  $C_{60}$  is small even under strong laser excitation, with the atom displacement far below the Lindemann criterion [44]. The global rotation of  $C_{60}$  generates several hundred of  $\hbar$ . Our finding here represents a different direction for phonon angular momentum research, and is expected to motivate experimental and theoretical investigations.

We define the total angular momentum of  $C_{60}$  as

$$\mathbf{J} = \sum_i \mathbf{j}_i(t) = \sum_i \mathbf{r}_i(t) \times \mathbf{p}_i(t), \quad (1)$$

where  $\mathbf{p}_i(t)$  is its momentum of atom  $i$  at time  $t$  and  $\mathbf{r}_i(t)$  is its position vector. The reason why we use  $\mathbf{J}$  instead of  $\mathbf{L}$  will become clear below. Although we do not quantize the atomic vibration formally here, we still use phonons below. To find the initial coordinates  $\{\mathbf{r}_i(0)\}$  of carbon atoms in  $C_{60}$ , we use the spiral generation method proposed by Fowler and Manolopoulos [45] for the topological problem of fullerenes. Here, in brief, we first construct the adjacency matrix, and diagonalize it. The three lowest eigenvectors correspond to the  $x$ ,  $y$ , and  $z$  coordinates of the carbon atoms, and then we properly rescale them according to the radius of  $C_{60}$ .

To optimize the geometry, we employ the Su-Schrieffer-Heeger (SSH) model [46] often used in conjugated polymers, where only  $\pi$  electrons are treated quantum mechanically, and the nuclear motions are described by the classical potentials [47] since the mass of carbon atoms is more than three orders of magnitude larger than that of the electron. Recently, the SSH model finds an important application in topological insulators [48]. The Hamiltonian reads [49–51]

$$H_0 = - \sum_{\langle ij \rangle, \sigma} t_{ij} c_{i, \sigma}^\dagger c_{j, \sigma} + \text{H.c.} + \frac{K_1}{2} \sum_{\langle ij \rangle} (r_{ij} - d_0)^2 + \frac{K_2}{2} \sum_i \delta\theta_{i,p}^2 + \frac{K_3}{2} \sum_i (\delta\theta_{i,h,1}^2 + \delta\theta_{i,h,2}^2), \quad (2)$$

where  $c_{i, \sigma}^\dagger$  is the electron creation operator at site  $i$  with spin  $\sigma (= \uparrow \downarrow)$  [52] and the summation  $\langle ij \rangle$  over  $i(j)$  runs from 1 to 60 with  $i \neq j$ . The first term on the right-hand side represents the electron hopping between nearest-neighbor atoms at positions  $\mathbf{r}_i$  and  $\mathbf{r}_j$ ,  $t_{ij} = t_0 - \alpha(|\mathbf{r}_i - \mathbf{r}_j| - d_0)$ , where  $r_{ij} = |\mathbf{r}_i - \mathbf{r}_j|$ ,  $t_0$  is the average hopping constant, and  $\alpha$  is the

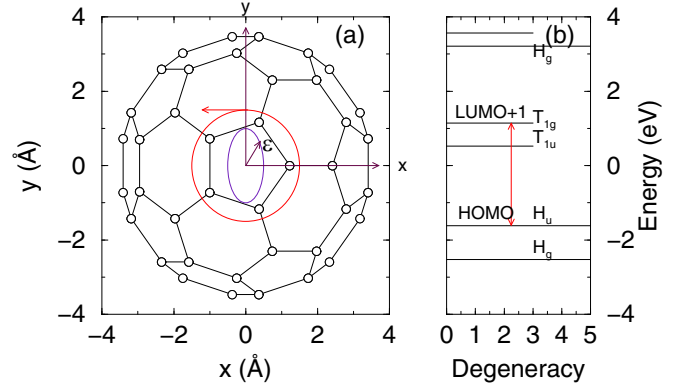


FIG. 1. (a)  $C_{60}$  structure. The empty circles denote 60 carbon atoms. The laser polarization (the vector) is in the  $xy$  plane (the front pentagon) and controlled by the helicity  $\epsilon$ . (b) Energy level scheme for  $C_{60}$ . The double arrow denotes the transition between the second lowest unoccupied molecular orbital (LUMO + 1) and the highest occupied molecular orbital (HOMO).

electron-lattice coupling constant. The last three terms are the lattice stretching, pentagon-hexagon, and hexagon-hexagon bending energies, respectively (see further details in [53]). You *et al.* [54] parametrized the Hamiltonian by fitting the energy gap, bond lengths, and 174 normal mode frequencies to their respective experimental values. They found that  $t_0 = 1.91$  eV,  $\alpha = 5.0$  eV/Å,  $K_1 = 42$  eV/Å<sup>2</sup>,  $K_2 = 8$  eV/rad<sup>2</sup>,  $K_3 = 7$  eV/rad<sup>2</sup>, and  $d_0 = 1.5532$  Å. These parameters are consistent with the literature values [55–62]. With You’s six parameters and with the electrons initially occupying 30 lowest energy levels, we optimize the structure. Figure 1(a) shows a two-dimensional structure of our optimized  $C_{60}$ , where the  $z$  axis is out of the page. The  $C_{60}$  molecule has the highest  $I_h$  point symmetry. 60 carbon atoms form 90 bonds, 60 single bonds around 12 pentagons, and 30 single bonds shared by 20 hexagons [see Fig. 1(a)]. Our double bond length is 1.403 Å, and the single bond length is 1.443 Å, both of which indeed match the experimental values of  $1.40 \pm 0.015$  Å and  $1.45 \pm 0.015$  Å [63,64]. Figure 1(b) shows the energy spectrum with the degeneracy. The highest occupied molecular orbital (HOMO) is a  $H_u$  state, while the lowest unoccupied molecular orbital (LUMO) is a  $T_{1u}$  state. The first dipole-allowed transition is between HOMO and LUMO + 1, which is highlighted by the double arrow. All these features are fully consistent with the prior study [54]. The challenge is to fit 174 normal mode frequencies [65] with only six parameters. We find that the calculated frequencies within our theory slightly deviate from the experimental values [65] within 3%. For instance, our breathing mode  $A_g(1)$  frequency is 481  $\text{cm}^{-1}$ , while the experimental one is between 492 [28] and 496 [65]  $\text{cm}^{-1}$ . Our pentagonal pinch mode  $A_g(2)$ ’s frequency is 1477  $\text{cm}^{-1}$ , while the experimental one is 1470 [28,65]  $\text{cm}^{-1}$ . Here the error is 0.5%. Because our Hamiltonian does not include high-order terms [66], these small differences are expected and do not affect our main conclusion of the Letter. For this reason, we do not adjust those parameters.

As seen above, there are varieties of ways to induce angular momentum change. We perturb the system with an ultrafast

laser pulse, whose interaction with  $C_{60}$  is described by

$$H_I = -e \sum_{i\sigma} \mathbf{E}(t) \cdot \mathbf{r}_i n_{i\sigma}, \quad (3)$$

where  $\mathbf{E}(t)$  is the electric field of the laser and  $n_{i\sigma}$  is the electron number operator at site  $i$ . We choose a Gaussian pulse for  $\mathbf{E}(t)$ :  $\mathbf{E}(t) = A_0 \exp(-t^2/\tau^2)[\cos(\omega t)\hat{x} + \epsilon \sin(\omega t)\hat{y}]/\sqrt{1+\epsilon^2}$ , where  $A_0$ ,  $\omega$ ,  $\tau$ ,  $t$ ,  $\epsilon$ , and  $\tau$  are the field amplitude, laser frequency, pulse duration or width, time, helicity, and pulse duration, respectively.  $\hat{x}$  and  $\hat{y}$  are the unit vectors along the  $x$  and  $y$  axes, respectively. We ensure that  $A_0$  is large enough, so the quantum effect of light is small and the classical treatment of our laser field is adequate. We treat the electrons quantum mechanically through the time-dependent Liouville equation [51,52],

$$i\hbar \frac{\partial \langle \rho_{ij}^\sigma \rangle}{\partial t} = \langle [H, \rho_{ij}^\sigma] \rangle, \quad (4)$$

where  $H = H_0 + H_I$ , and  $\rho_{ij}^\sigma$  is the density matrix. The lattice vibrations are described by the Newtonian equation. This classical treatment of nuclear motion is reasonable if the de Broglie wavelength is smaller than the system size, but if the de Broglie wavelength becomes comparable to the system size, then our approach is less accurate. We solve the coupled Liouville and Newtonian equations numerically.

We excite  $C_{60}$  with a 60-fs laser pulse with electric field amplitude of  $0.01 \text{ V/\AA}$ . The photon energy is  $2.76 \text{ eV}$ , which is tuned to be resonant with the transition between HOMO and LUMO + 1 [see Fig. 1(b)]. Figure 2(a) displays the total energy (thin line), lattice kinetic energy (thick line), and lattice potential energy (thick dashed line) as a function of time. The curve around zero denotes the laser pulse. Upon laser excitation, energy enters the electronic system first. The peak in the total energy is mainly due to the electron energy. Through the electron-lattice interaction and laser excitation, the lattice starts to vibrate. Most of the lattice energy is in the potential energy, and the kinetic energy is very small. In the figure, we multiply the kinetic energy by 100. Carbon atoms move at a speed of  $10^{-3}$ – $10^{-2} \text{ \AA/fs}$ , or 100–1000 m/s, very typical for nuclear vibrations. The oscillation is due to the energy exchange between the electron and lattice subsystems (for details, see [53]). Since we want to check the energy conservation as well as vibrational oscillations, we do not dampen our system. We find that the oscillation has a period of 69.3 fs, which exactly matches the frequency of the breathing mode  $A_g(1)$  [67,68]. Such a coherent phonon excitation has been observed experimentally [67] and in other systems as well [43]. The reason why this  $A_g(1)$  is excited strongly is due to our chosen laser parameters [50,53]. Our interest is in the lattice angular momentum. Figure 2(b) shows the lattice angular momentum for three laser helicities ( $\epsilon$ ): right ( $\sigma^+$ ), left ( $\sigma^-$ ), and linear ( $\pi$ ) pulses, with the polarization in the  $xy$  plane [see Fig. 1(a)]. There is a general trend as to how the angular momentum is transferred to the lattice. Upon laser excitation, the flow of angular momentum to the lattice occurs on the 100 fs timescale, which corresponds to the total energy absorbed. Although each atom still vibrates and exchanges its angular momentum with the rest of the atoms, the total angular momentum must remain constant and is conserved in the absence of an external field. This is rigorously reproduced

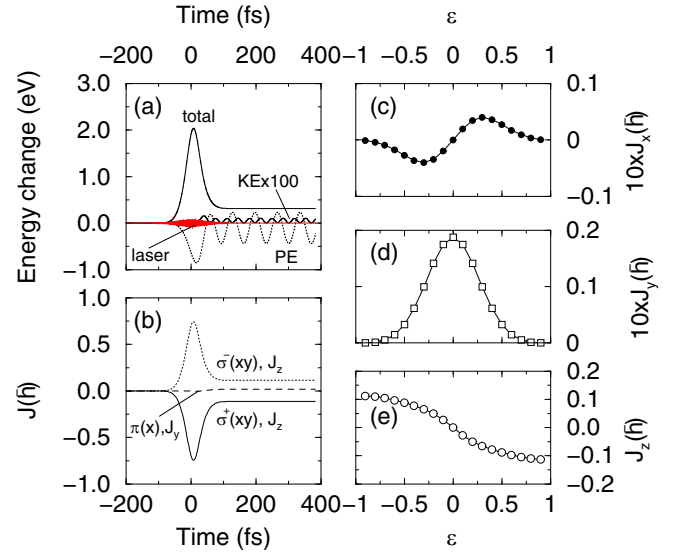


FIG. 2. (a) Total energy change as a function of time under a 60-fs  $\sigma^+$  pulse. Here  $\epsilon = 1$ . The laser field amplitude is  $0.01 \text{ V/\AA}$ , and the photon energy is  $\hbar\omega = 2.76 \text{ eV}$ . Thin solid, thick solid, and dashed lines denote the system total energy, lattice kinetic energy, and potential energy, respectively. The lattice kinetic energy is multiplied by 100 to have an easy view. To demonstrate the energy conservation, the system is not damped. The red thin line around 0 is the laser electric field. The oscillation period in the lattice potential is 69.3 fs, which exactly matches the frequency of the Raman-active  $A_g(1)$  mode. (b) Total angular momentum  $\mathbf{J}$  under  $\sigma^+$  (solid line),  $\sigma^-$  (dotted line), and  $\pi$  pulses (dashed line). Only the strongest component of  $\mathbf{J}$  is shown. Linearly polarized light transfers a small angular momentum. The left- and right-circularly polarized light transfer opposite angular momenta. All the pulses have the same laser parameters as (a). (c), (d), and (e) show the final  $x$ ,  $y$ , and  $z$  components of  $\mathbf{J}$  as a function of ellipticity  $\epsilon$ .

in our calculation. The angular momentum shows a strong dependence on  $\epsilon$ . For  $\sigma^-$ , the lattice angular momentum is along the  $+z$  axis, while for  $\sigma^+$ , it is along the  $-z$  axis. The  $\pi$  pulse induces a much weaker angular momentum (see the long-dashed line). This is expected because the angular momentum of light is directly related to the helicity of light. When it interacts with  $C_{60}$ , the lattice angular momentum has the hallmark of incident light. Figures 2(c)–2(e) show the detailed change in  $J_x$ ,  $J_y$ , and  $J_z$  as a function of helicity  $\epsilon$ . When  $\epsilon = 0$ , the laser polarization is linear along the  $x$  axis. One can see that only  $J_y$  differs from zero, because the atom moves mainly along the  $x$  axis. Going from  $\epsilon = 0$  to 1, our pulse changes from a linearly polarized pulse to elliptically, and finally to a circularly polarized pulse. Both  $J_x$  and  $J_z$  increase significantly as the atom also moves along the  $y$  axis.  $J_z$  is negative as expected. When we change  $\epsilon$  from 0 to  $-1$ , we have a left elliptically to circularly polarized pulse, so  $J_z$  flips its sign, fully consistent with our finding in Fig. 2(b).

What is unknown or less familiar is whether and how the lattice angular momentum  $\mathbf{J}$  can characterize a system. This is an important conceptual question because angular momentum is rarely used to characterize the dynamics of a system, except in atoms and some simple structures. Prior studies [9,11–14] are all based on this assumption. We compare  $\mathbf{J}$  against the

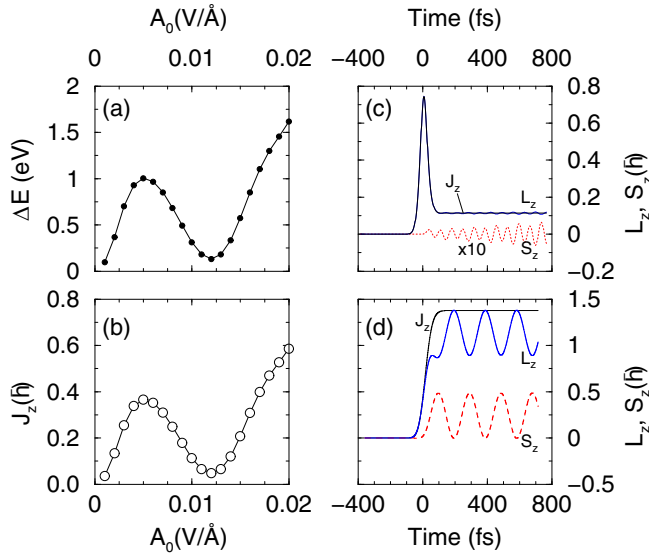


FIG. 3. (a) Absorbed energy  $\Delta E$  as a function of laser field amplitude  $A_0$ . The photon energy and pulse duration are the same as Fig. 2. (b) Total angular momentum as a function of laser field amplitude  $A_0$ , which matches the total energy change. This demonstrates that  $\mathbf{J}$  is physical. (c) The orbital  $L_z$  and spin  $S_z$  angular momenta as a function of time.  $S_z$  is very small when  $\hbar\omega = 2.76$  eV. In the figure, it is multiplied by 10. (d) The orbital  $L_z$  and spin  $S_z$  angular momenta as a function of time with  $\hbar\omega = 0.185$  eV.  $S_z$  reaches a comparable magnitude as  $L_z$ . The dependence of  $S_z$  on time follows a sine function, while that of  $L_z$  follows a cosine function, very similar to DECP [43].

absorbed energy  $\Delta E$  into  $C_{60}$ . When the laser photon energy is off resonance, the energy change follows the perturbative path and has a simple dependence on the laser field amplitude  $A_0$  [69], so the agreement between the angular momentum  $\mathbf{J}$  and  $\Delta E$  could be coincidental. The harder question is what happens if the laser is on resonance. Figure 3(a) shows the energy absorbed as a function of laser field amplitude where the photon energy is tuned to the dipole-allowed transition between the HOMO and LUMO + 1 states [Fig. 1(b)]. It is clear that the dependence on  $A_0$  is highly nonlinear. When  $A_0$  is far below 0.005 V/Å, the change is linear, but as far as it closes to 0.005 V/Å, it peaks, after which it starts to decrease. Because resonant excitation activates multiple real electronic excitation, this opens other channels and  $\Delta E$  decreases. Once  $A_0$  exceeds 0.01 V/Å,  $\Delta E$  increases again, which is consistent with our prior study [49]. Figure 3(b) is our angular momentum. One can see that its change with  $A_0$  matches the absorbed energy change, down to some minor details. This proves that  $\mathbf{J}$  is physical, and it represents the acquired angular momentum from light.

It has been proposed that if one rewrites  $\mathbf{r}(t)$  as a sum of the equilibrium position  $\mathbf{r}_i(0)$  and the displacement  $\mathbf{u}_i(t)$ ,  $\mathbf{r}_i(t) = \mathbf{r}_i(0) + \mathbf{u}_i(t)$ , the angular momentum for atom  $i$  can be separated into two terms:

$$\mathbf{j}_i(t) = \mathbf{r}_i(0) \times \mathbf{p}_i(t) + \mathbf{u}_i(t) \times \mathbf{p}_i(t) \equiv \mathbf{l}_i(t) + \mathbf{s}_i(t). \quad (5)$$

$\mathbf{l}_i(t)$  is called the orbital angular momentum of atom  $i$ , while  $\mathbf{s}_i(t)$  is called the spin angular momentum [3,9,10,12] because  $\mathbf{s}_i$  is independent of the initial position of an atom. By

separating orbital from spin angular momentum, we can directly investigate the interplay between spin and orbital angular momenta on an ultrafast timescale.

Figure 3(c) compares the spin angular momentum with the orbital counterpart. We employ a 60-fs laser pulse with  $\hbar\omega = 2.76$  eV and  $A_0 = 0.01$  V/Å. We notice that the angular momentum mainly enters the orbital part. From Eq. (5), we see that it is the momentum  $\mathbf{p}_i$  that is mainly responsible for this increase.  $S_z$  is very small and magnified by 10 in the figure. What is interesting is that the spin angular momentum does not follow the laser pulse, very different from the orbital angular momentum. The reason for this difference is straightforward.  $S_z$  depends on both  $\mathbf{u}_i(t)$  and  $\mathbf{p}_i$ . Although the pulse peaks at 0 fs, the atom cannot follow instantaneously and needs time to respond. The behavior of  $L_z$  is like a cosine function, with its maximum at 0 fs, similar to dispersive excitation of coherent phonons (DECPs) [43]. But  $S_z$  is like a sine function. The sum of  $S_z$  and  $L_z$  is  $J_z$ , which is constant after the laser field is gone because the system does not have a way to exchange angular momentum. This demonstrates that our definition of angular momentum through Eq. (5) is physically sound.

It has been a big challenge to induce phonon spin angular momentum in real materials [19,21,22]. We can increase spin angular momentum by tuning the laser photon energy to vibrations directly [17]. We choose  $\hbar\omega = 0.185$  eV, or 44.7 THz, to be resonant with nuclear vibrations. The laser pulse duration is also 60 fs and the field amplitude is increased to 0.15 V/Å. We caution that our current treatment of nuclear vibration may not be adequate to compute the infrared spectrum since we do not include the nuclear dipole moment and the nuclear vibration is not treated quantum mechanically. Figure 3(d) shows that  $S_z$  reaches  $0.5\hbar$ . Under our laser field, the structure of  $C_{60}$  is well maintained, far below the Lindemann criterion [44] for melting. This criterion has been a major obstacle for a prior study [19], where the atomic displacements for BaO and LiNbO<sub>3</sub> can be as large as 0.1 Å. Therefore, an experimental test is difficult.

The top figure of Fig. 4 shows atomic displacements projected on the  $xy$  plane for five atoms on the front pentagon. The scales for the  $x$  and  $y$  axes are increased by 100 for an easy view. One can see the displacement is well below the Lindemann criterion. This paves the way to experimental testing. What is even more interesting is that besides these internal rotations, under thermal excitation, the entire molecule spins rapidly, although along arbitrary axes at room temperature. The angular momentum is  $L = I\Omega$ , where  $I$  is the moment of inertia of  $C_{60}$  and  $\Omega$  is the angular speed. Assuming  $C_{60}$  spins along the  $z$  axis through two pentagons (see Fig. 1), the moment of inertia is  $I_z = m \sum_{i=1}^{60} (x_i^2 + y_i^2)$ , where  $m$  is the mass of carbon atom and  $x_i$  and  $y_i$  are the coordinates of atom  $i$ . Note that the moment of inertia is almost identical along other axes because  $C_{60}$  is highly spherical. An early estimate puts  $\Omega$  between 1.5/ps and 2.8/ps [70]. According to the latest theoretical estimate [29], its average angular frequency is 0.34 rad/ps. Since our present study only contains one single  $C_{60}$  and has no intermolecular interaction between several fullerenes, we are unable to verify their average angular frequency. Instead, we use their number and find  $|\mathbf{J}|$  for  $C_{60}$  to be  $322\hbar$ . This angular momentum is from the global rotation



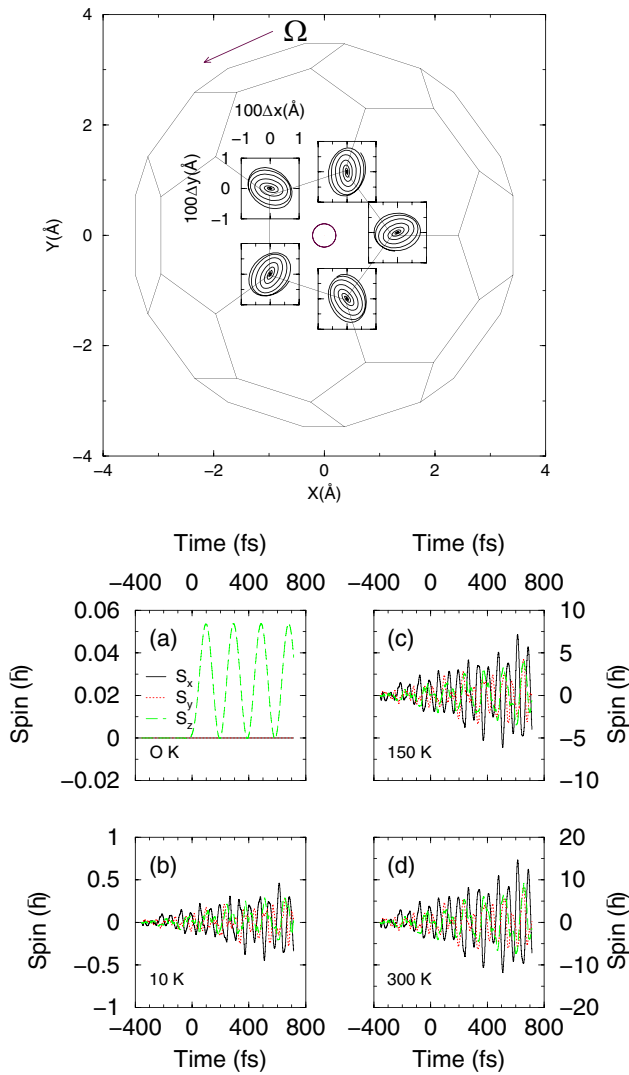


FIG. 4. Top: Traces of displacements of five carbon atoms on the front pentagon in the earlier stage of laser excitation. The change is only  $0.01 \text{ \AA}$ , which is well below the Lindemann criterion [44]. The arrow on the top left denotes the rotation of entire  $C_{60}$ . Bottom: Phonon spin angular momentum at (a) 0 K, (b) 10 K, (c) 150 K, and (d) 300 K, where the solid, dotted, and long-dashed lines denote  $S_x$ ,  $S_y$ , and  $S_z$ , respectively. Its magnitude becomes larger as temperature increases.

of  $C_{60}$ . Because our Hamiltonian in Eq. (2) only depends on the distance between neighboring atoms, the rapid global rotation of  $C_{60}$  does not enter our calculation directly and only implicitly through the laser field polarization. However, due to the high symmetry of  $C_{60}$ , different polarizations yield almost identical results. Therefore, the global rotation must be treated separately in our formalism. To see the thermal effect of the global rotation on the spin angular momentum, we set the initial velocities of the carbon atoms to  $\sqrt{k_B T/m}$ , where  $k_B$  is the Boltzmann constant and  $m$  is the carbon mass. We allow

a random distribution of the initial velocity directions. We use four temperatures,  $T = 0, 10, 150,$  and  $300 \text{ K}$ .

The results are shown in the bottom figures of Fig. 4. Figure 4(a) is our result with 0 K, but with a small laser field amplitude of  $0.01 \text{ V/\AA}$ . The solid, dotted, and long-dashed lines denote  $S_x$ ,  $S_y$ , and  $S_z$ , respectively, and are the same for the rest of the figures. We see that only  $S_z$  has a sizable value. But as we increase temperature to 10 K, we find that all the other components are increased to  $0.5\hbar$ . The amplitude is comparable among all three components. At 150 K, the spin increases to  $5\hbar$ . At room temperature of 300 K, Fig. 4(d) shows the spin angular momentum increases to  $10\hbar$ . We also check whether our initial configuration of velocity direction affects our results. Among all the configurations we investigate, we do not see any qualitative difference. They should be observable experimentally. Spinning  $C_{60}$  could be a natural phonon angular momentum generator. As a large group of other fullerenes are available and even its endohedral forms already exist, such as  $N@C_{60}$  and  $P@C_{60}$ , our finding opens a route to phonon angular momentum. The future study should focus on how to harvest such a huge momentum for technological applications.

In conclusion, we have proposed a route to generate phonon orbital and spin angular momenta from  $C_{60}$ , without resorting to more complicated synthetic methods [18,19,21,22]. We show that a single laser pulse can transfer a significant amount of angular momentum to  $C_{60}$ . The phonon angular momentum that  $C_{60}$  receives shows a strong dependence on laser helicity. The circularly polarized light injects more momentum than the linearly polarized light. We demonstrate that the total angular momentum change follows the total energy change faithfully, thus establishing that even in the time domain PAM is a valid concept and can be used to characterize the system property. The orbital angular momentum is normally larger than the spin counterpart, and it also has a different dependence on time. Similar to DECP [43], the orbital has a cosine function dependence, while the spin has a sine function dependence. We find that the atomic displacement is spiral and its amplitude is far below the Lindemann criterion, which has been a big obstacle to a prior study [19]. The angular momentum of the entire  $C_{60}$  reaches  $322\hbar$  at room temperature. Since endohedral fullerenes such as  $N@C_{60}$  and  $P@C_{60}$  are readily available, our study points out a large group of materials suitable for phonon angular momentum generation. It is expected that our finding will motivate experimental and theoretical investigations in this field and beyond.

This work was solely supported by the U.S. Department of Energy under Contract No. DE-FG02-06ER46304. Part of the work was done on Indiana State University's high performance Quantum and Obsidian clusters. The research used resources of the National Energy Research Scientific Computing Center, which is supported by the Office of Science of the U.S. Department of Energy under Contract No. DE-AC02-05CH11231.

- [1] T. Brixner, J. Stenger, H. M. Vaswani, M. Cho, R. E. Blankenship, and G. R. Fleming, Two-dimensional spectroscopy of electronic couplings in photosynthesis, *Nature (London)* **434**, 625 (2005).
- [2] F. Gai, K. C. Hasson, J. C. McDonald, and P. A. Anfinrud, Chemical dynamics in proteins: The photoisomerization of retinal in bacteriorhodopsin, *Science* **279**, 1886 (1998).
- [3] D. A. Garanin and E. M. Chudnovsky, Angular momentum in spin-phonon processes, *Phys. Rev. B* **92**, 024421 (2015).
- [4] M. Föhnle, Th. Tsatsoulis, C. Illg, M. Haag, B. Y. Müller, and L. Zhang, Ultrafast demagnetization after femtosecond laser pulses: Transfer of angular momentum from the electronic system to magnetoelastic spin-phonon modes, *J. Supercond. Nov. Magn.* **30**, 1381 (2017).
- [5] D. Zahn, F. Jakobs, Y. W. Windsor, H. Seiler, T. Vasileiadis, T. A. Butcher, Y. Qi, D. Engel, U. Atxitia, J. Vorberger, and R. Ernstorfer, Lattice dynamics and ultrafast energy flow between electrons, spins, and phonons in a 3d ferromagnet, *Phys. Rev. Research* **3**, 023032 (2021).
- [6] S. Coh, Classification of materials with phonon angular momentum and microscopic origin of angular momentum, [arXiv:1911.05064](https://arxiv.org/abs/1911.05064).
- [7] S. V. Vonsovskii and M. S. Svirskii, Phonon spin, *Sov. Phys. Solid State* **3**, 1568 (1962).
- [8] A. D. Levine, A note concerning the spin of the phonon, *Nuovo Cimento* **26**, 190 (1962).
- [9] L. Zhang and Q. Niu, Angular Momentum of Phonons and the Einstein–de Haas Effect, *Phys. Rev. Lett.* **112**, 085503 (2014).
- [10] A. G. McLellan, Angular momentum states for phonons and a rotationally invariant development of lattice dynamics, *J. Phys. C: Solid State Phys.* **21**, 1177 (1988).
- [11] J. J. Nakane and H. Kohno, Angular momentum of phonons and its application to single-spin relaxation, *Phys. Rev. B* **97**, 174403 (2018).
- [12] A. Rückriegel and R. A. Duine, Long-Range Phonon Spin Transport in Ferromagnet-Nonmagnetic Insulator Heterostructures, *Phys. Rev. Lett.* **124**, 117201 (2020).
- [13] S. Park and B.-J. Yang, Phonon angular momentum Hall effect, *Nano Lett.* **20**, 7694 (2020).
- [14] S. Streib, Difference between angular momentum and pseudoangular momentum, *Phys. Rev. B* **103**, L100409 (2021).
- [15] K. Moseni, R. Wilson, and S. Coh, Electric field control of phonon angular momentum in perovskite BaTiO<sub>3</sub>, [arXiv:2103.06316](https://arxiv.org/abs/2103.06316).
- [16] M. Hamada, E. Minamitani, M. Hirayama, and S. Murakami, Phonon Angular Momentum Induced by the Temperature Gradient, *Phys. Rev. Lett.* **121**, 175301 (2018).
- [17] A. Stupakiewicz, C. S. Davies, K. Szerenos, D. Afanasiev, K. S. Rabinovich, A. V. Boris, A. Caviglia, A. V. Kimel, and A. Kirilyuk, Ultrafast phononic switching of magnetization, *Nat. Phys.* **17**, 489 (2021).
- [18] L. Zhang and Q. Niu, Chiral Phonons at High-Symmetry Points in Monolayer Hexagonal Lattices, *Phys. Rev. Lett.* **115**, 115502 (2015).
- [19] D. M. Juraschek and N. A. Spaldin, Orbital magnetic moments of phonons, *Phys. Rev. Materials* **3**, 064405 (2019).
- [20] O. Bistoni, F. Mauri, and M. Calandra, Intrinsic Vibrational Angular Momentum from Nonadiabatic Effects in Noncollinear Magnetic Molecules, *Phys. Rev. Lett.* **126**, 225703 (2021).
- [21] T. F. Nova, A. Cartella, A. Cantaluppi, M. Först, D. Bossini, R. V. Mikhaylovskiy, A. V. Kimel, R. Merlin, and A. Cavalleri, An effective magnetic field from optically driven phonons, *Nat. Phys.* **13**, 132 (2017).
- [22] J. Holanda, D. S. Maior, A. Azevedo, and S. M. Rezende, Detecting the phonon spin in magnon-phonon conversion experiments, *Nat. Phys.* **14**, 500 (2018).
- [23] S. Streib, H. Keshtgar, and G. E. W. Bauer, Damping of Magnetization Dynamics by Phonon Pumping, *Phys. Rev. Lett.* **121**, 027202 (2018).
- [24] K. An *et al.*, Coherent long-range transfer of angular momentum between magnon Kittel modes by phonons, *Phys. Rev. B* **101**, 060407(R) (2020).
- [25] A. Rückriegel, S. Streib, G. E. W. Bauer, and R. A. Duine, Angular momentum conservation and phonon spin in magnetic insulators, *Phys. Rev. B* **101**, 104402 (2020).
- [26] H. W. Kroto, J. R. Heath, S. C. O'Brien, R. F. Curl, and R. E. Smalley, C<sub>60</sub>: Buckminsterfullerene, *Nature (London)* **318**, 162 (1985).
- [27] R. D. Johnson, C. S. Yannoni, H. C. Dorn, J. R. Salem, and D. S. Bethune, C<sub>60</sub> rotation in the solid state: Dynamics of a faceted spherical top, *Science* **255**, 1235 (1992).
- [28] M. S. Dresselhaus, G. Dresselhaus, and P. C. Eklund, *Science of Fullerenes and Carbon Nanotubes* (Academic, San Diego, California, 1996).
- [29] A. M. Bubenchikov, M. A. Bubenchikov, D. V. Mamontov, and A. V. Lun-Fu, MD-simulation of fullerene rotations in molecular crystal fullerite, *Crystals* **9**, 496 (2019).
- [30] R. Tycko, R. C. Haddon, G. Dabbagh, S. H. Glarum, D. C. Douglass, and A. M. Muzsice, Solid-state magnetic resonance spectroscopy of fullerenes, *J. Phys. Chem.* **95**, 518 (1991).
- [31] R. Tycko, G. Dabbagh, R. M. Fleming, R. C. Haddon, A. V. Makhija, and S. M. Zahurak, Molecular Dynamics and the Phase Transition in Solid C<sub>60</sub>, *Phys. Rev. Lett.* **67**, 1886 (1991).
- [32] L.-L. Wang and H.-P. Cheng, Rotation, translation, charge transfer, and electronic structure of C<sub>60</sub> on Cu(111) surface, *Phys. Rev. B* **69**, 045404 (2004).
- [33] S. I. Bozhko, S. A. Krasnikov, O. Lübben, B. E. Murphy, K. Radican, V. N. Semenov, H. C. Wu, B. Bulfin, and I. Shvets, Rotational transitions in a C<sub>60</sub> monolayer on the WO<sub>2</sub>/W(110) surface, *Phys. Rev. B* **84**, 195412 (2011).
- [34] N. Neel, L. Limot, J. Kröger, and R. Berndt, Rotation of C<sub>60</sub> in a single-molecule contact, *Phys. Rev. B* **77**, 125431 (2008).
- [35] Y. Zou, B. Liu, L. Wang, D. Liu, S. Yu, P. Wang, T. Wang, M. Yao, Q. Li, B. Zou, T. Cui, G. Zou, T. Wagberg, B. Sundqvist, and H.-K. Mao, Rotational dynamics of confined C<sub>60</sub> from near-infrared Raman studies under high pressure, *Proc. Natl. Acad. Sci. USA* **106**, 22135 (2009).
- [36] J. R. F. Lima, J. Brandao, M. M. Cunha, and F. Moraes, Effects of rotation in the energy spectrum of C<sub>60</sub>, *Eur. Phys. J. D* **68**, 94 (2014).
- [37] R. Saito, G. Dresselhaus, and M. S. Dresselhaus, Hindered rotation of solid <sup>12</sup>C<sub>60</sub> and <sup>13</sup>C<sub>60</sub>, *Phys. Rev. B* **50**, 5680 (1994).
- [38] D. S. Bethune, R. D. Johnson, J. R. Salem, M. S. de Vries, and C. S. Yannoni, Atoms in carbon cages: The structure and properties of endohedral fullerenes, *Nature (London)* **366**, 123 (1993).
- [39] J. Hernandez-Rojas, J. Breton, and J. M. G. Llorente, Rotational dynamics of endohedral C<sub>60</sub> fullerene complexes, *J. Phys. Chem. Solids* **58**, 1689 (1997).

- [40] R. B. Ross, C. M. Cardona, D. M. Guldi, S. G. Sankaranarayanan, M. O. Reese, N. Kopidakis, J. Peet, B. Walker, G. C. Bazan, E. Van Keuren, B. C. Holloway, and M. Drees, Endohedral fullerenes for organic photovoltaic devices, *Nat. Mater.* **8**, 208 (2009).
- [41] J. Twamley, Quantum-cellular-automata quantum computing with endohedral fullerenes, *Phys. Rev. A* **67**, 052318 (2003).
- [42] M. Mitrano, A. Cantaluppi, D. Nicoletti, S. Kaiser, A. Perucchi, S. Lupi, P. Di Pietro, D. Pontiroli, M. Ricc , S. R. Clark, D. Jaksch, and A. Cavalleri, Possible light-induced superconductivity in  $K_3C_{60}$  at high temperature, *Nature (London)* **530**, 461 (2016).
- [43] H. J. Zeiger, J. Vidal, T. K. Cheng, E. P. Ippen, G. Dresselhaus, and M. S. Dresselhaus, Theory for dispersive excitation of coherent phonons, *Phys. Rev. B* **45**, 768 (1992).
- [44] F. A. Lindemann,  ber die Berechnung molekularer Eigenfrequenzen, *Phys. Z.* **11**, 609 (1910).
- [45] P. W. Fowler and D. E. Manolopoulos, *An Atlas of Fullerenes* (Clarendon, Oxford, 1995).
- [46] W. P. Su, J. R. Schrieffer, and A. J. Heeger, Solitons in Polyacetylene, *Phys. Rev. Lett.* **42**, 1698 (1979).
- [47] A. J. Heeger, S. Kivelson, J. R. Schrieffer, and W. P. Su, Solitons in conducting polymers, *Rev. Mod. Phys.* **60**, 781 (1988).
- [48] J. K. Asboth, L. Oroszlany, and A. Palyi, *A Short Course on Topological Insulators: Band Structure and Edge States in One and Two Dimensions*, Lecture Notes in Physics Vol. 919 (Springer, New York, 2016).
- [49] G. P. Zhang, X. Sun, and T. F. George, Laser-induced ultrafast dynamics in  $C_{60}$ , *Phys. Rev. B* **68**, 165410 (2003).
- [50] G. P. Zhang and T. F. George, Controlling Vibrational Excitations in  $C_{60}$  by Laser Pulse Durations, *Phys. Rev. Lett.* **93**, 147401 (2004).
- [51] G. P. Zhang, Optical High Harmonic Generations in  $C_{60}$ , *Phys. Rev. Lett.* **95**, 047401 (2005).
- [52] G. P. Zhang, Hartree-Fock Dynamical Electron-Correlation Effects in  $C_{60}$  after Laser Excitation, *Phys. Rev. Lett.* **91**, 176801 (2003).
- [53] See Supplemental Material at <http://link.aps.org/supplemental/10.1103/PhysRevB.104.L100302> for the following three sections. The first section provides the details of our Hamiltonian. Figure 1 shows the convention of our angular terms. The used parameters are provided in Table I. The detailed expression of the normal mode calculation is listed. Table II shows the computed normal mode frequencies. The second section is on the thermal effect. Table III lists the angular momentum for three temperatures. The third section is on the energy exchange between the lattice and electron subsystems (see Fig. 2) and the energy and angular momentum change as a function of time (see Fig. 3).
- [54] W. M. You, C. L. Wang, F. C. Zhang, and Z. B. Su, Application of a Su-Schrieffer-Heeger-like model to the intramolecular electron-phonon coupling in  $C_{60}$  clusters, *Phys. Rev. B* **47**, 4765 (1993).
- [55] G. B. Adams, J. B. Page, O. F. Sankey, K. Sinha, J. Menendez, and D. R. Huffman, First-principles quantum molecular-dynamics study of the vibrations of icosahedral  $C_{60}$ , *Phys. Rev. B* **44**, 4052(R) (1991).
- [56] M. Menon and K. R. Subbaswamy, Universal Parameter Tight-Binding Molecular Dynamics: Application to  $C_{60}$ , *Phys. Rev. Lett.* **67**, 3487 (1991).
- [57] J. L. Feldman, J. Q. Broughton, L. L. Boyer, D. E. Reich, and M. D. Kluge, Intramolecular-force-constant model for  $C_{60}$ , *Phys. Rev. B* **46**, 12731 (1992).
- [58] J. C. R. Faulhaber, D. Y. K. Ko, and P. R. Briddon, Vibronic coupling in  $C_{60}$  and  $C_{60}^{3-}$ , *Phys. Rev. B* **48**, 661 (1993).
- [59] B. Friedman, Infrared absorption of polarons in  $C_{60}$ , *Phys. Rev. B* **48**, 17551 (1993).
- [60] K. Harigaya and S. Abe, Optical-absorption spectra in fullerenes  $C_{60}$  and  $C_{70}$ : Effects of Coulomb interactions, lattice fluctuations, and anisotropy, *Phys. Rev. B* **49**, 16746 (1994).
- [61] W.-Z. Wang, C.-L. Wang, Z.-B. Su, and L. Yu, Lattice Relaxation Study on Self-Trapped Exciton and Biexciton in Neutral and Charged Fullerenes, *Phys. Rev. Lett.* **72**, 3550 (1994).
- [62] J. Liu, S. Iwata, and B. Gu, Structural properties of the endohedral complex  $Na^+@C_{60}$ , *J. Phys.: Condens. Matter* **6**, L253 (1994).
- [63] K. Hedberg, L. Hedberg, D. S. Bethune, C. A. Brown, H. C. Dorn, R. D. Johnson, and M. de Vries, Bond lengths in free molecules of Buckminsterfullerene,  $C_{60}$ , from gas-phase electron diffraction, *Science* **254**, 410 (1991).
- [64] C. S. Yannoni, P. P. Bernier, D. S. Bethune, G. Meijer, and J. R. Salem, NMR determination of the bond lengths in  $C_{60}$ , *J. Am. Chem. Soc.* **113**, 3190 (1991).
- [65] J. Menendez and J. B. Page, Vibrational spectroscopy of  $C_{60}$ , in *Light Scattering in Solids VIII: Fullerenes, Semiconductor Surfaces, Coherent Phonons*, edited by M. Cardona and G. G ntherodt (Springer, New York, 2000).
- [66] Z. C. Wu, D. A. Jelski, and T. F. George, Vibrational motions of Buckminsterfullerene, *Chem. Phys. Lett.* **137**, 291 (1987).
- [67] S. L. Dexheimer, D. M. Mittleman, R. W. Schoenlein, W. Vareka, X.-D. Xiang, A. Zettl, and C. V. Shank, Ultrafast dynamics of photoexcited  $C_{60}$ , in *Ultrafast Pulse Generation and Spectroscopy*, edited by T. R. Gosnell, A. J. Taylor, K. A. Nelson, and M. C. Downer, SPIE Proc. 1861 (SPIE-International Society for Optical Engineering, Bellingham, WA, 1993), p. 328.
- [68] G. P. Zhang and T. F. George, Normal-mode selectivity in ultrafast Raman excitations in  $C_{60}$ , *Phys. Rev. B* **73**, 035422 (2006).
- [69] Y. R. Shen, *The Principles of Nonlinear Optics* (Wiley, Hoboken, New Jersey, 2003).
- [70] Q.-M. Zhang, J.-Y. Yi, and J. Bernholc, Structure and Dynamics of Solid  $C_{60}$ , *Phys. Rev. Lett.* **66**, 2633 (1991).